Optics Communications 556 (2024) 130297

Contents lists available at ScienceDirect

Optics Communications

journal homepage: www.elsevier.com/locate/optcom

High efficiency and ultra-wideband water-based microwave absorber using 3D printing

Huu Lam Phan [a,b], Dac Tuyen Le [c], Xuan Khuyen Bui [d], Dinh Lam Vu [e], Hong Quang Nguyen [g], Ngoc Huyen Duong [f], Thi Minh Nguyen [g], Thi Quynh Hoa Nguyen [g,h,*], Jung-Mu Kim [h,**]

[a] Laboratory for Computational Mechanics, Institute for Computational Science and Artificial Intelligence, Van Lang University, Ho Chi Minh City, 70000, Vietnam
[b] Faculty of Mechanical - Electrical and Computer Engineering, School of Technology, Van Lang University, Ho Chi Minh City, 70000, Vietnam
[c] Department of Physics, Hanoi University of Mining and Geology, 18 Pho Vien, Hanoi, 10000, Vietnam
[d] Institute of Materials Sciences, Vietnam Academy of Science and Technology, 18 Hoang Quoc Viet, Hanoi, 10000, Vietnam
[e] Graduate University of Science and Technology, Vietnam Academy of Science and Technology, 18 Hoang Quoc Viet, Hanoi, 10000, Vietnam
[f] Faculty of Electrical Engineering Technology, Industrial University of Ho Chi Minh City, 12 Nguyen Van Bao , Ho Chi Minh city, 70000, Vietnam
[g] School of Engineering and Technology, Vinh University, 182 Le Duan, Vinh city, 46000, Vietnam
[h] Department of Electronic Engineering, Jeonbuk National University, Jeonju, 54896, Republic of Korea

ARTICLE INFO

Keywords:
Water-based absorber
Metamaterials
Broadband
3D printing
Microwave

ABSTRACT

Ultra-wideband water-based microwave metasurface absorbers have attracted considerable interest owing to their promising applications for electromagnetic radiation prevention and stealth technology, etc. Here, we propose a high-efficiency and ultra-wideband water-based metasurface absorber, consisting of a periodically truncated cone water-filled containers made by 3D printed polylactic acid (PLA) resin, which can realize an absorption rate above 90% and a relative bandwidth of up to 154.5% in the frequency band from 6.5 GHz to 50.7 GHz. This absorber can work at a wide angle of incidence and polarization insensitivity and reveals superior thermal stability. Moreover, the proposed absorber is reconfigurable for tunable absorption by controlling the water content and type of inside liquids. The performance of the proposed structure is verified by experiment, which shows a good agreement with the simulation result. Due to the excellent features such as ultra-wideband absorption, low cost, and environmentally friendly materials, the proposed water-based metasurface absorber can be applied in the fields of electromagnetic stealth and radiation protection.

1. Introduction

Electromagnetic (EM) absorbing devices are nowadays enormously applied in various fields such as stealth technologies [1–3], solar energy harvesting [4,5], and thermal emitters [6]. The disadvantages of traditional absorbers, such as bulky devices and poorly absorbed efficiency, significantly restrict their practical usage [7]. Recently, metamaterials (MMs) or metasurfaces (MSs), which are three-dimensional (3D) or two-dimensional (2D) arrays including sub-wavelength artificial building blocks, have demonstrated their compact size and design freedom in the desired manipulation of the EM wave [8]. As a result, metamaterial absorbers (MMAs) have drawn a lot of attention because of their extraordinary properties, such as ultra-thin and high absorption efficiency. Landy et al. reported a perfect absorber made of MMs in 2008 [9], which consisted of an artificial sub-wavelength metallic pattern array deposited on a dielectric layer and a metallic sheet. Inspired by the first MMA, studies on MMAs concentrated on the ultra-thin metallic structure have been implemented to achieve strong absorption via enhancing impedance match [10–12]. Nevertheless, the significant resonance dispersion of these kinds of MMAs results in a narrowed bandwidth. Since then, many attempts have been propounded to expand the absorption bandwidth of MMAs. For example, the multilayer structures which achieved a wideband MMA were reported [13–15]. These designs could stimulate multi-frequency resonant absorption modes to enlarge significantly their absorption bandwidth. Unfortunately, this approach caused a complexity in the fabrication process regarding high cost and time-consuming. Another approach based on a combination of various-sized resonant unit cells in a plane has also extended the bandwidth of MMAs [16,17]. However, this method has some functional constraints, such as polarization-dependency and sensitivity to the oblique incidence [18]. Furthermore, the resonant metal layer is usually fractured, oxidized, and corroded, which is limited usage [19]. To overcome the aforementioned shortcomings, an

* Corresponding author at: School of Engineering and Technology, Vinh University, 182 Le Duan, Vinh city, 46000, Vietnam.
** Corresponding author at: Department of Electronic Engineering, Jeonbuk National University, Jeonju, 54896, Republic of Korea.
E-mail addresses: ntqhoa@vinhuni.edu.vn (T.Q.H. Nguyen), jungmukim@jbnu.ac.kr (J.-M. Kim).

https://doi.org/10.1016/j.optcom.2024.130297
Received 15 December 2023; Received in revised form 8 January 2024; Accepted 10 January 2024
Available online 13 January 2024

all-dielectric material structure was proposed to broaden the bandwidth and achieve better absorption performance [20]. In the all-dielectric structure, the dielectric loss mainly contributes to the absorption of the EM wave. Thus, a high dielectric loss metamaterial could be a viable option for perfect absorption over a wide frequency range.

Water is an abundant and bio-compatible material in life. In addition, water has a dispersive permittivity and large dielectric loss at microwave frequencies [21,22]. As a result, it can be used in MMA design to attain broadband absorption. One publication related to water-based MMA was reported by Yoo et al. in 2015 [23]. They created periodic water droplets on a surface of one substrate by controlling surface wettability to widen the absorption band up to 8–18 GHz. However, it was difficult to maintain the water droplet structure for a long period due to the gravity effect, which caused its functional limitation in practical application. To overcome the problem, the water containers in the water-based MMAs structure were applied by using 3D-printing technology. By this way, Huang et al. proposed a cross-shaped water container in the water-based MMA structure that achieved a broad absorption band from 8.1 GHz to 22.9 GHz [24]. Shen et al. demonstrated their water-based MMA using an irregular shape with a large absorption band of 6.8–21 GHz [25]. Similarly, Zhou et al. presented an I-shaped water-based MMA that obtained an absorption band of 7.9–21.7 GHz [26]. In 2020, Zhang et al. reported a water-based MMA relied on a swastika-shaped water container to expand an absorption band from 9.3 GHz to 49 GHz [27]. Although the above water containers printed by 3D printing technology can easily control the water content, these MMAs have still worked at a narrow band or a narrow incident angle. Recently, Kwon et al. showed an MMA based on water-based moth-eye structures that extended an absorption band from 4 GHz to 120 GHz, corresponding with a relative bandwidth (RBW) of 187% However, the thickness of the designed water-based structure is quite thick, and it is difficult to realize in a practical application. Furthermore, there is little information about the significant correlations between resin properties such as dielectric constant and loss tangent, which eventually affect the absorption efficiency as well as the operation frequency range of the proposed structure.

Herein, we propose a high-efficiency and ultra-wideband water-based metasurface absorber (UWBWMA) based on a truncated cone-shaped water container fabricated using 3D printing technology. The proposed structure can obtain an absorption efficiency above 90% over a frequency range of 6.5–50.7 GHz with an RBW of 154.5%. Importantly, our proposed structure can maintain its performance with the various resin properties of the 3D printing resin material, indicating that this design can be easily fabricated by conventional 3D printers. Furthermore, the proposed UWBWMA is reconfigurable for tunable absorption by tailoring the water content and type of inside liquids.

2. Structure design and method

A schematic of the proposed water-based absorber using 3D printing technology is illustrated in Fig. 1. A unit cell structure includes a truncated cone water container, which is placed inside a 3D-printed polylactic acid (PLA) cylinder shell, a cross-shaped channel, and a continuous copper ground plane. The permittivity and loss-tangent of 3D-printed PLA is 2.6 and 0.03, respectively. The copper layer has a conductivity σ of 4.56×10^7 S/m and a thickness t of 0.035 mm. Meanwhile, the frequency-dependent permittivity of water can be calculated by the Debye formula [25,28,29]:

$$\epsilon(\omega) = \epsilon_\infty(\omega, T) + \frac{\epsilon_s(\omega, T) - \epsilon_\infty(\omega, T)}{1 - i\omega\tau(\omega, T)} \quad (1)$$

where temperature $T = 25$ °C, epsilon infinity $\epsilon_\infty = 3.1$, epsilon static $\epsilon_s(\omega, T) = 78.4$ and the relaxation time $\tau(\omega, T) = 8.27 \times 10^{-12}$ s.

In this study, the finite difference frequency domain (FDFD) solver of CST Microwave Studio software is utilized to design and evaluate the absorption performance of the proposed UWBWMA. In the simulation setup, the unit cell boundary conditions are specified for the x- and y-directions, while the z-direction is set to open (add space) boundary conditions. Furthermore, the normal incident EM wave propagating from the positive z-axis on the surface to the inside structure and the tetrahedral mesh type are selected. Based on the simulation, the unit cell geometrical parameters of the UWBWMA are optimized to achieve high efficiency and wideband characteristics. The final dimensions of the designed UWBWMA are found to be $W = 200$ mm, $P = 11.4$ mm, $D = 9$ mm, $a = 7$ mm, $b = 3$ mm, $h_1 = 1$ mm, $h_2 = 3.5$ mm, $h_3 = 1.4$ mm, $c = 1$ mm, and $s = 0.8$ mm, as depicted in Fig. 1(b) and (c), respectively.

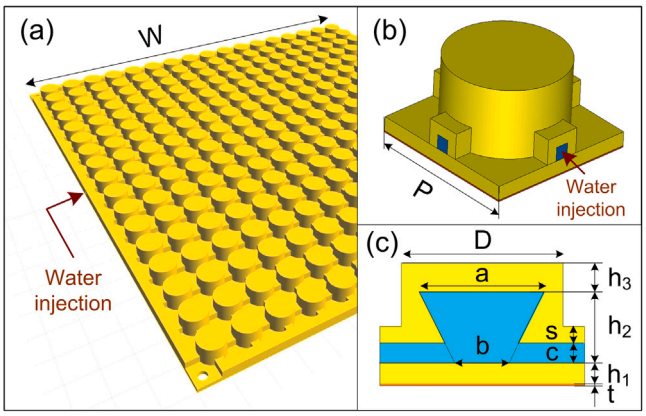

Fig. 1. The schematic view of a unit-cell of the proposed UWBWMA: (a) 3D-view, (b) a unit-cell, (c) cross-section view.

In our design, the truncated cone water-filled container acts as the main resonator for absorption. To calculate the absorption ($A(\omega)$) of the proposed structure, we use Eq. (2) [9,30]:

$$A(\omega) = 1 - R(\omega) - T(\omega) \quad (2)$$

where reflection $R(\omega) = |r_{yy}|^2 + |r_{xy}|^2$, transmission $T(\omega) = |t_{yy}|^2 + |t_{xy}|^2$, and "$yy$" and "$xy$" represent co-and cross-polarization components, respectively. Because the copper bottom layer is substantially thicker than the skin depth of the incident wave, which can obstruct the transmission wave ($T(\omega) = 0$). Therefore, the absorption is calculated through the reflective coefficient as $A(\omega) = 1 - R(\omega)$.

Furthermore, the absorption performance is frequently evaluated through the RBW, which is calculated as Eq. (3) [30].

$$RBW = 2 \times \frac{f_H - f_L}{f_H + f_L} \quad (3)$$

where f_H and f_L are the highest and lowest frequency with absorption over 90%.

3. Results and discussion

Fig. 2 shows the simulated absorption, transmission, and reflection efficiency of the proposed UWBWMA for normal incident wave interaction. It is clear that the UWBWMA shows a high absorption efficiency of over 90% in the ultra-wideband frequency range of 6.5–50.7 GHz, corresponding to an absorption bandwidth of 44.2 GHz and an RBW of 154.5%. At the frequencies of 7.42 GHz, 12.85 GHz, and 48.5 GHz, the absorptance can approximately reach up to 100%. This demonstrates that the proposed absorber realizes high-efficiency and ultra-wideband absorption characteristics.

To further assess the absorption performance of the UWBWMA, the effect of the incidence and the polarization angles on the absorption spectra under both transverse electric (TE) and transverse magnetic (TM) polarizations is studied. Fig. 3 illustrates the contour map of the absorption efficiency versus the oblique, polarization incident angles, and frequency under the TE and TM modes, respectively. For a TE mode, the absorptance decreases with the increase of the incident

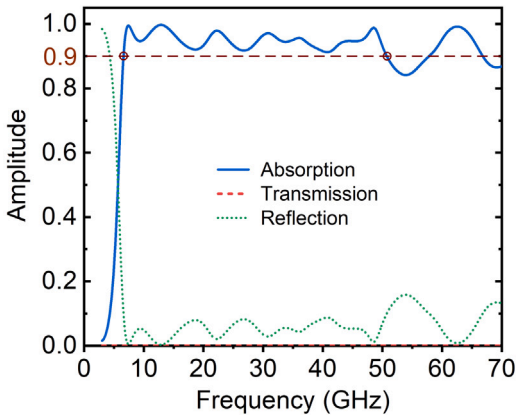

Fig. 2. Absorption, transmission, and reflection spectra of the proposed UWBWMA.

angle; however, it can still attain above 90% and 80% in the operating bandwidth when the incident angle is up to 40° and 50°, respectively, as depicted in Fig. 3(a) and (c). For the TM mode, the absorption rates are maintained higher than 90% with an incident angle in the range from 0° to 50°. Further increasing the incident angle up to 60°, the absorptance can remain higher than 80% in the whole working band, as shown in Fig. 3(b) and (d). It was reported that the absorptance difference when changing the incident angles between the TE and TM modes is due to magnetic field orientation [31]. For the TM mode, when increasing the incident angle, the magnetic field direction is almost unchanged, which powerfully controls the induced currents at all incident angles. This ensures that the impedance matching is maintained at all incidence angles. In contrast to the TM mode, the magnetic field direction varies with the different incident angles, causing inadequate induced current and decreased magnetic flux in the structure for the TE mode. Thus, the absorption efficiency for TE polarization is less than that at TM mode under large incident angles. Meanwhile, under both TE and TM modes, the absorption spectra of the proposed UWBWMA are unchanged with the changing of the polarization angles because of its symmetric structure, as illustrated in Fig. 3(e) and (f), respectively. These observations confirm that the proposed UWBWMA is insensitive to the incident and polarization angles under both TE and TM modes.

To analyze the absorption mechanism, the impedance matching theory is used to explain the perfect absorption of the proposed structure. When incident EM waves normally impinged on a water-based absorber, the equivalent complex impedance (Z) can be expressed as Eq. (4) [32–34].

$$Z = \sqrt{\frac{(1+S_{11})^2 - S_{21}^2}{(1-S_{11})^2 - S_{21}^2}} = \frac{1+S_{11}}{1-S_{11}} \tag{4}$$

where, S_{11} and S_{21} are the reflection and transmission coefficients, respectively. In the instance of satisfying the impedance matching conditions, the equivalent complex impedance is approximately 1. Due to the outstanding dispersion properties of water in the microwave band, the equivalent impedance of the water-based absorber can be maintained over a large bandwidth. To verify the abovementioned, the normalized impedance of the proposed UWBMMA is calculated, as shown in Fig. 4. It can be seen that the real part of the impedance is close to 1, while the imaginary part is approximately zero in the operating frequency range of 6.5 GHz–50.7 GHz. It implies that the impedance matching can be obtained in the whole working band, resulting in achieving near-unity absorbance in the proposed UWBMMA.

To further explore the mechanism of the proposed water-based absorber metasurface, the distributions of electric field, magnetic field, and energy loss at the three absorption peaks of 7.42 GHz, 12.85 GHz, and 48.5 GHz are presented in Fig. 5, respectively. The electric field is distributed mostly in the surrounding region of the water and the resin shell at the three peaks, as shown in Fig. 5(a), (b), and (c). Meanwhile, at the resonant frequency of 7.42 GHz, the magnetic field distribution is mainly localized on the bottom-middle part of the water-filled inside container, while the electric field distribution is almost non-existent in the same space, as in Fig. 5(d). It was reported that this spatial separation of electric and magnetic fields at 7.42 GHz is due to the presence of standing waves [35,36]. Similarly, a quite similar phenomenon can be observed at the frequency of 12.85 GHz. In addition, there exist two other regions of magnetic field distribution, which are concentrated near the bottom edges of the water layer, at this frequency, as shown in Fig. 5(e). In contrast, it is predominantly situated between the upper water layer and the resin shell at the higher resonant frequency of 48.5 GHz, as illustrated in Fig. 5(f). The power loss is concentrated in the water-filled inside of the proposed water-based absorber for three resonant frequencies. At a low frequency of 7.42 GHz, the power loss is harvested in the upper central part of the water layer and the entire area of the channels (Fig. 5(g)). The power loss at 12.85 GHz is focused on inside the channels and the areas from the edge part to the central part of the water layer (Fig. 5(h)). Meanwhile, the power loss is located in the upper part of the water layer at 48.5 GHz (Fig. 5(i)). It demonstrates that the power loss of the structure is mainly caused by water in the container. From the above observation, we see that the electric resonance is created by the interaction of water and its resin shell. Meanwhile, the magnetic resonance is mainly formed in the water, which causes the power loss energy of the EM wave. It indicates that the power loss distributions at these frequencies are due to the effect of magnetic loss [37]. Therefore, the resonance frequency of 7.42 GHz is affected by magnetic loss and the presence of standing waves, while higher resonance frequencies of 12.85 GHz and 48.5 GHz are mainly affected by magnetic loss. Due to the contribution of magnetic resonance, the proposed structure shows more angular resistance with increasing the incident angle in TM mode than that of the TE mode.

The influences of the 3D printing resin material properties of dielectric constant (ϵ_r) and loss tangent (δ) on the absorption performance are characterized. As seen from Fig. 6(a) and (b), the absorption spectra of the water-based absorber are slightly varied with the changing of dielectric constant in the range from 2.4 to 3.2 and loss tangent in the range of 0.02 to 0.06. However, the absorbance drops below 90% at around 27 GHz when reducing the ϵ_r below 2.4 and the bandwidth starts to shrink slightly at the high-frequency region around 50 GHz with increasing ϵ_r (Fig. 6(a)). Meanwhile, there exists a tendency for the absorption to grow better with the increase of the loss tangent in the whole bandwidth of 6.5–50.7 GHz, as shown in Fig. 6(b). Therefore, our designed structure can be suitable for fabricating by conventional 3D printing resin materials without reducing its performance.

In the practical application, the function of an absorber device is transferring EM energy to thermal energy. This causes the varying temperature of the water. The temperature change leads to the variation of the dielectric constant of the water as described by Debye formula (Eq. (1)). Based on Debye formula, the dielectric permittivity of water at different temperatures is calculated and illustrated in the inset of 6(c). It can be seen that both real and imaginary parts of the dielectric permittivity of water change significantly with temperature, which may influence the absorption performance of the water-based absorber. However, it was recently reported that the water-based MM absorber is insensitive to temperature [26] and explained that the reason for such a stable absorption performance should be the structural design of the water-based absorber [26]. Thus, it is essential to investigate the influence of the temperature versus the absorptance of the proposed structure. In this investigation, the influence of the variation of water temperature (from 0 °C to 100 °C) on the shell and metal properties of the water-based structure is ignored. Fig. 6(c) depicts the absorption spectrum with the different temperatures in the range from 0 °C to 100 °C. It is clear that the absorptive curve slightly changes under different temperatures. This implies that the absorption rate is almost

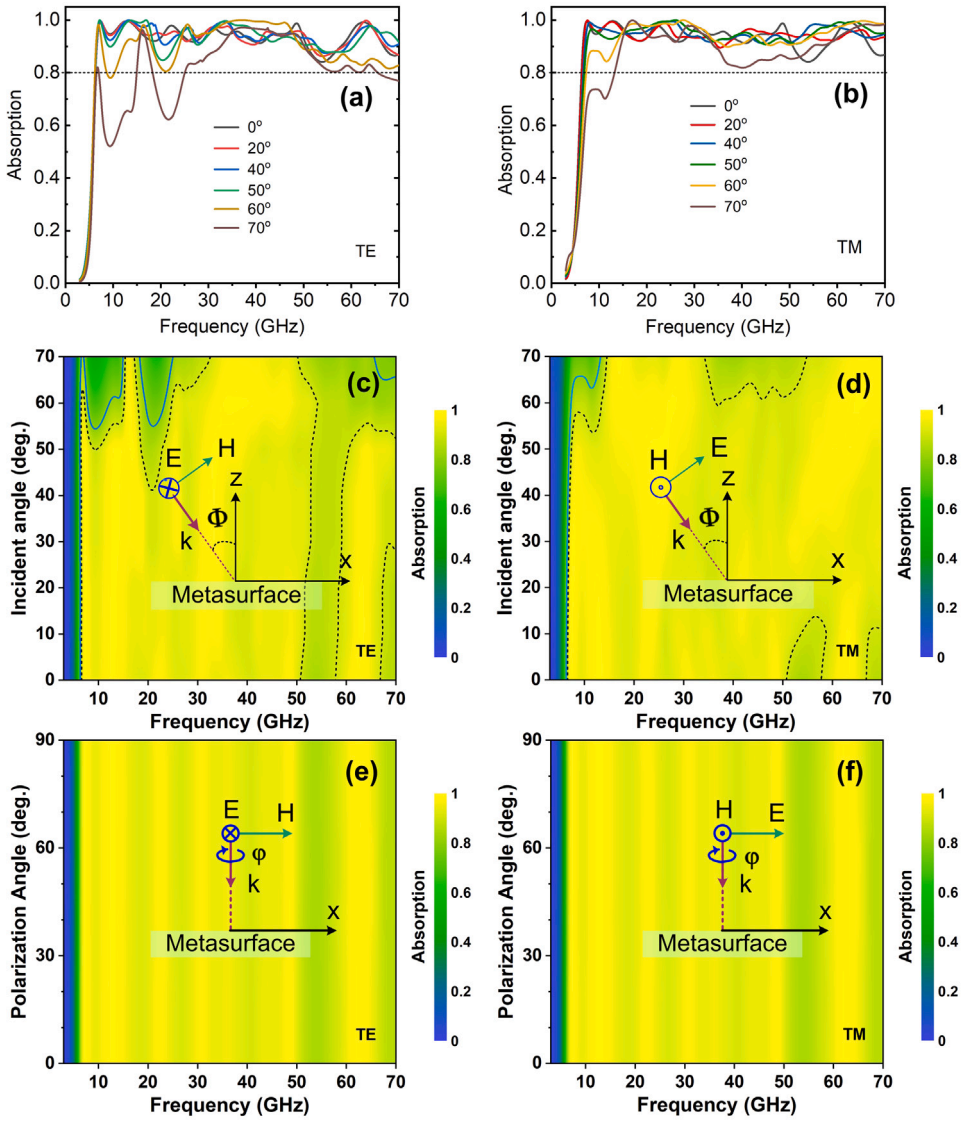

Fig. 3. Absorption efficiencies of the proposed UWBWMA as a function of (a)–(d) incident angle and (e), (f) polarization angle under TE and TM modes, respectively. In (a) and (b) plot the absorptivity lines at the selected incident angles and in (c) and (d) plot the blue solid and dash black contour curves indicated the 80% and 90% absorptivity, respectively.

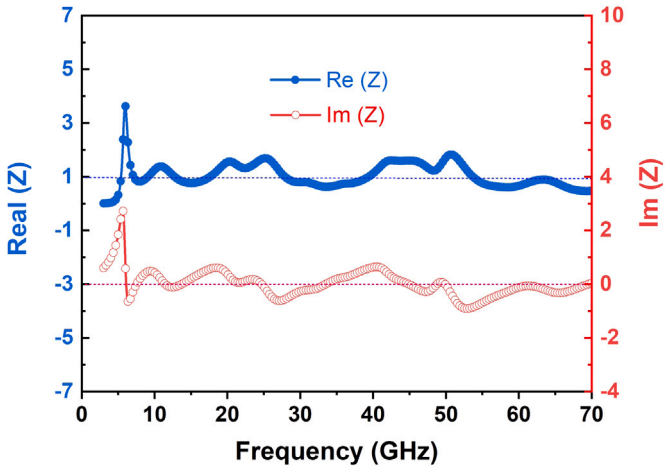

Fig. 4. Normalized impedance of the proposed UWBWMA.

maintained above 90% in the whole working band at different temperatures. Therefore, the suggested absorber structure can work stably when the temperature varies dramatically.

We have also analyzed the effect of different types of filling liquids such as methanol and ethanol on the absorbance of the proposed structure. The dielectric dispersion properties of methanol and ethanol liquids are calculated following the Debye model with $\epsilon_\infty = 5.3$, $\epsilon_s(\omega, T) = 32.6$, $\tau(\omega, T) = 46.8 \times 10^{-12}$ s and $\epsilon_\infty = 3.9$, $\epsilon_s(\omega, T) = 23.7$, $\tau(\omega, T) = 145.1 \times 10^{-12}$ s, respectively. Fig. 6(d) shows the absorption performance with the various filling liquids. When the container is filled with methanol or ethanol, the proposed structure also exhibits an absorption rate above 90% over wideband frequency. However, the edge of the operating bandwidth is shifted to a higher frequency. For the methanol-filled container and the ethanol-filled container of the proposed absorber, these absorption bandwidths are obtained in the range of 15–70 GHz and 20–30 GHz and 45–70 GHz, respectively.

Furthermore, the effect of the water level filled in the container on the absorptance of the designed UWBWMA is also investigated. Fig. 7 presents the variation of the absorption performance with respect to

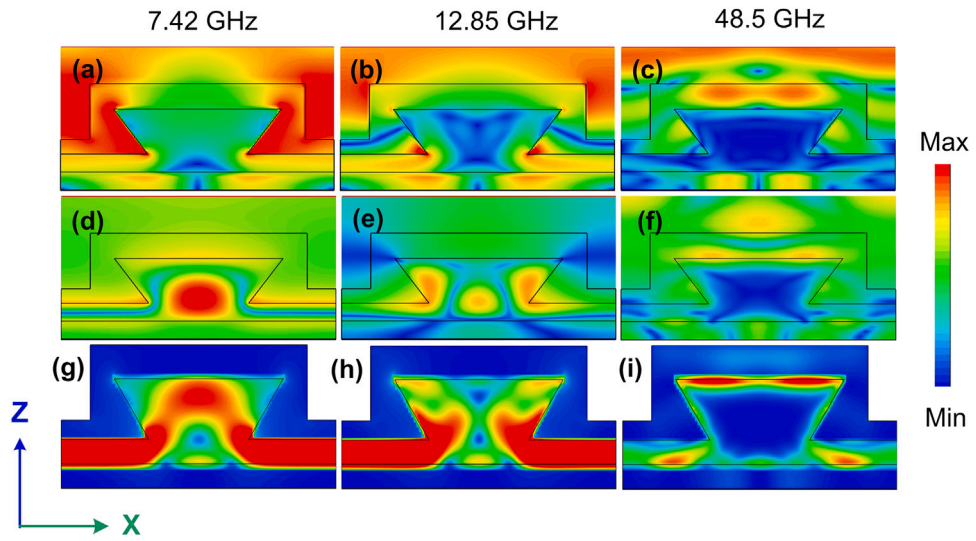

Fig. 5. (a)–(c) Electric field, (d)–(f) magnetic field, and (g)–(i) power loss energy distribution in a unit cell at various resonant frequencies of 7.42, 12.85 and 48.5 GHz in the XZ-plane, respectively.

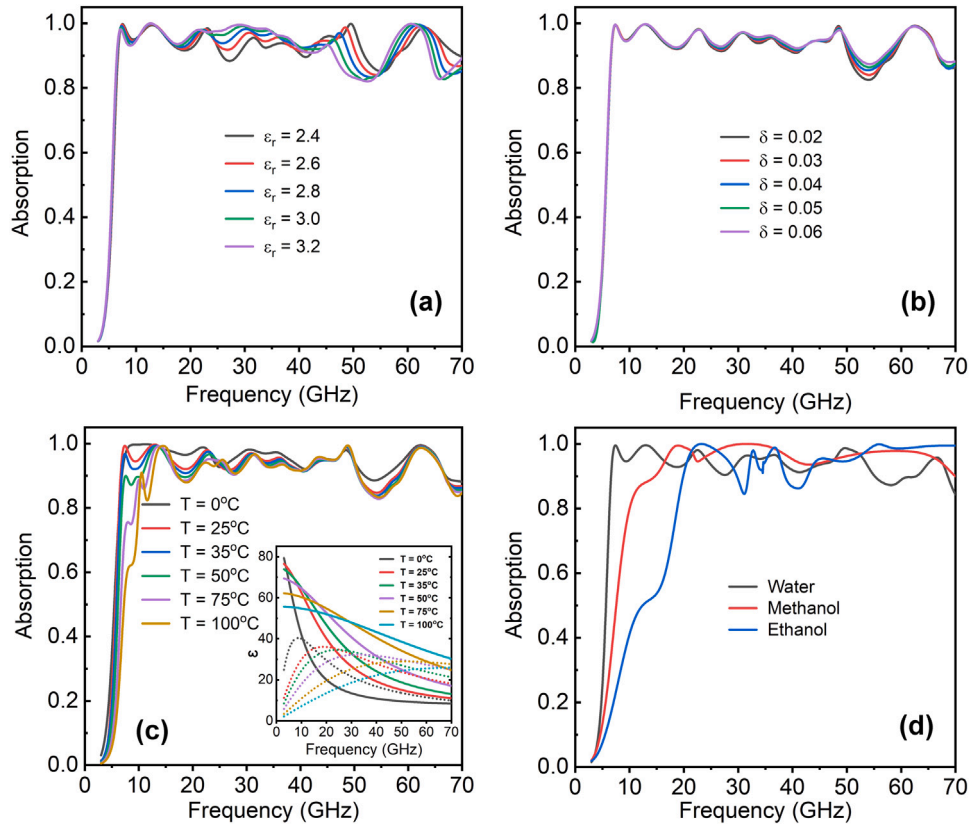

Fig. 6. Absorption spectra of the proposed UWBWMA with various 3D printing resin properties of (a) dielectric constant and (b) loss tangent, (c) different temperatures, and (d) other liquids. The inset in Fig. 6(c) is the dielectric permittivity of water as a function of frequency for temperature in the range of 0 °C to 100 °C (solid and dashed lines correspond to the real and imaginary parts, respectively).

the water level. When reducing the water level in the container to zero, the absorptance is significantly decreased, specifically in the frequency range below 20 GHz. At higher frequencies above 34 GHz, only a few discrete absorption peaks are observed and the wideband absorption feature of the designed UWBWMA is disappeared. When the water level gradually increases, the discontinuous absorption bandwidths are established with the absorption rate above 90%. With the full water level, the ultra-wideband absorption response can be obtained in the range from 6.5 GHz to 50.7 GHz. Based on the above analysis, it proves that the absorption response of the proposed UWBWMA can be tailored by turning the water level filled inside the container.

To analyze the influence of manufacturing errors, the absorption spectra are simulated by changing the structural parameters of P, D, a, b, h_1, h_2, and h_3 (see Fig. 1). Due to the fabrication error of the commercial 3D-printing such as Flashforge Creator 3 in the z-direction of ±0.4 mm and x-, y-directions of ±0.2 mm. Therefore, the structure

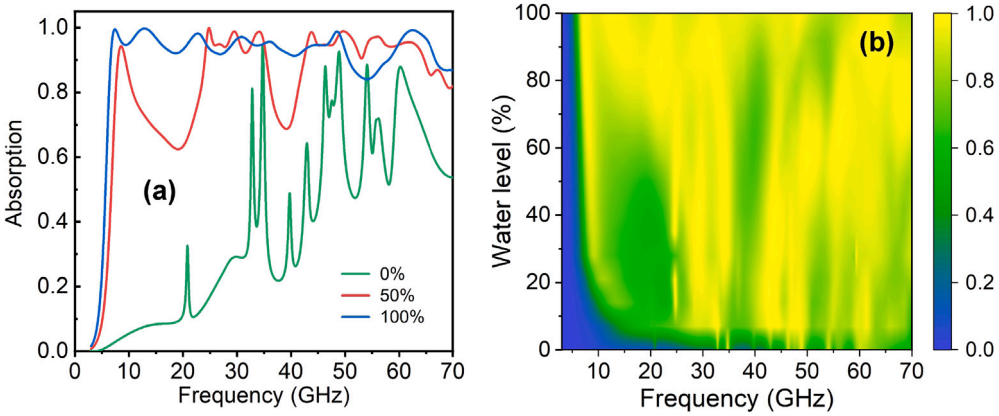

Fig. 7. (a) Absorption spectra and (b) Contour map of the proposed UWBWMA with different water levels.

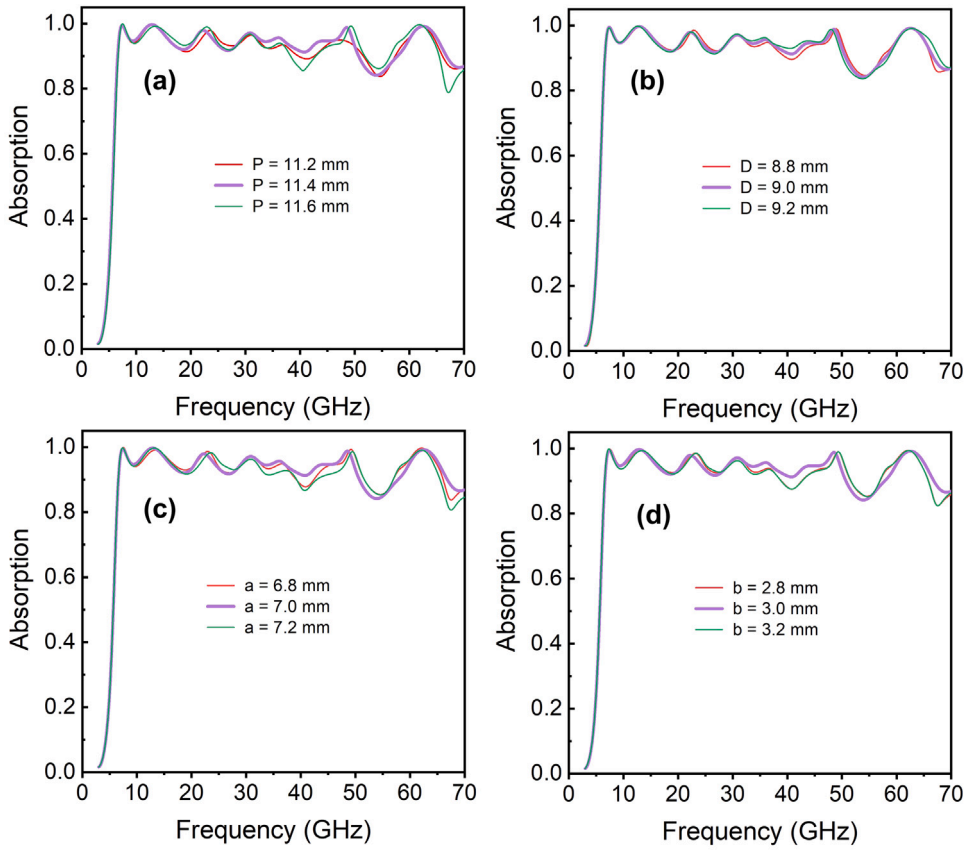

Fig. 8. Influence of structural parameters on absorption performance of the proposed UWBWMA: (a) P, (b) D, and (c) a, and (d) b.

parameters are investigated within these error ranges. Figs. 8 and 9 depict the simulated absorption when a single geometric parameter is varied with the fixed other parameters. As seen in Fig. 8, the absorption spectra are almost unchanged except at an absorption peak of around 40.6 GHz. However, the absorption performance is changed with varying thicknesses of h_1, h_2, and h_3, as illustrated in Fig. 9. The absorption efficiency is decreased with increasing of h_1 and decreasing of h_3 in the frequency range above 23 GHz, as seen in Fig. 9(a) and (c), respectively. Meanwhile, with increasing the h_2, the absorption efficiency is decreased in the frequency range below 38 GHz, while it is increased in the frequency range above 38 GHz (Fig. 9(b)). It means that the absorption performance of the proposed structure is slightly influenced by manufacturing errors of the parameters of P, D, a, b and relatively influenced by manufacturing errors of the parameters of h_1, h_2, and h_3.

4. Experimental verification

First, we fabricate the proposed structure with an overall size of 200 mm × 200 mm (17 × 17 unit cells), which corresponds to the same parameter in the simulation, using a 3D printer (Flashforge Creator 3). Then, the 3D-printed sample is attached to the copper layer of the FR4 substrate by four screws. The final fabricated sample is shown in Fig. 10(a). To verify the simulation result, the absorption spectrum of fabricated UWBWMA is measured using a vector network analyzer (VNA) (Rohde and Schwarz ZNB20) with two identical linearly polarized standard gain horn antennas (transmitting and receiving antennas). Due to the frequency limitation of our VNA, the measurement data is collected in the range of 3–18 GHz. The distance between the horn antennas and the sample (d) is 0.6 m and the spacing

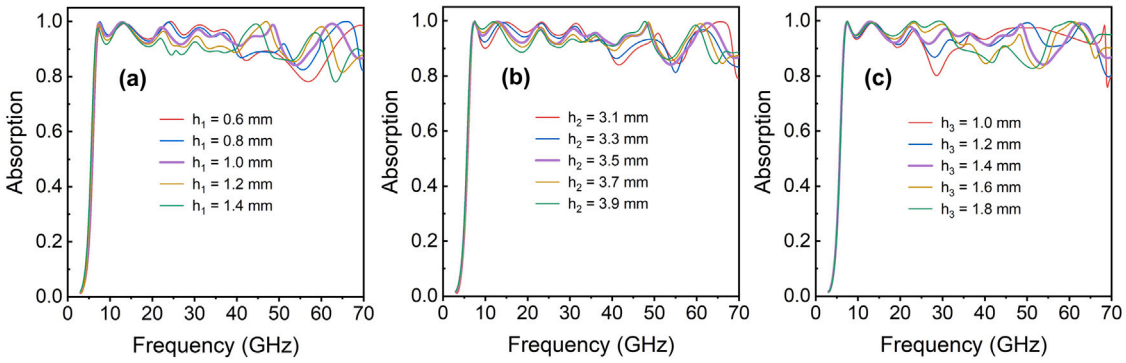

Fig. 9. Absorption spectra for various thickness structural parameters: (a) h_1, (b) h_2, and (c) h_3.

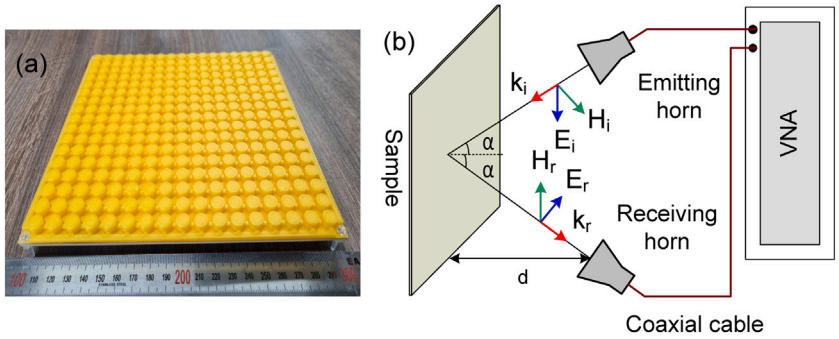

Fig. 10. (a) Photograph of the fabricated UWBWMA and (b) schematic diagram of the measurement setup.

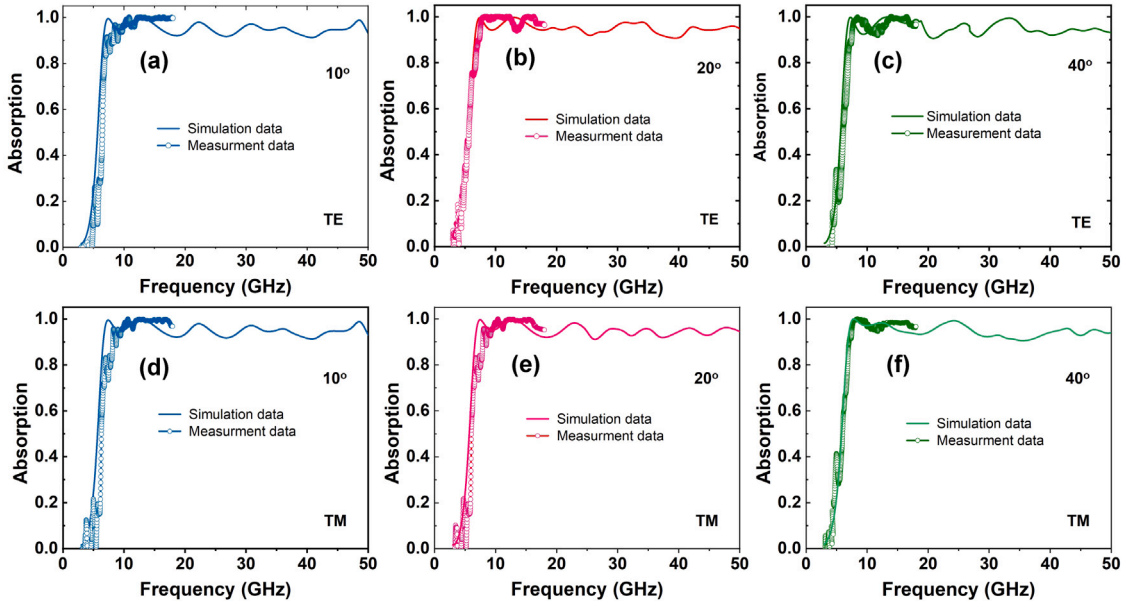

Fig. 11. The simulated and measured results of absorption spectra of the proposed UWBWMA under different incident angles of (a), (d) 10°, (b), (e) 20°, and (c), (f) 40° for TE and TM modes, respectively.

angle between two antennas is calibrated to be 10°, corresponding to the normal incidence measurement in the experimental setup. The measurement is taken at room temperature (25 °C) in the free space without the microwave anechoic chamber, therefore the measurement system is calibrated with this condition to embed the effect of the environment. The schematic diagram of the experiment setup is displayed in Fig. 10(b). For the calibration in our measurement, the copper plate (the same size as the fabricated sample) is assumed to be a perfect reflector and established at the same position as sample. The reference signal is obtained by measured value EM wave reflected by copper plate (perfect-reflecting body). Then, the absorption amplitude is estimated from the reflection difference between the sample and the copper plate.

Fig. 11 shows the measured absorption spectrum at various incident angles for both TE and TM modes. It can be seen that there is a good agreement between measured and simulated results for both TE and TM modes. The bandwidth of the fabricated sample shows an absorption rate above 90% in the range of the investigated frequency region with increasing the incident angle up to 40°, which proves the wide incident

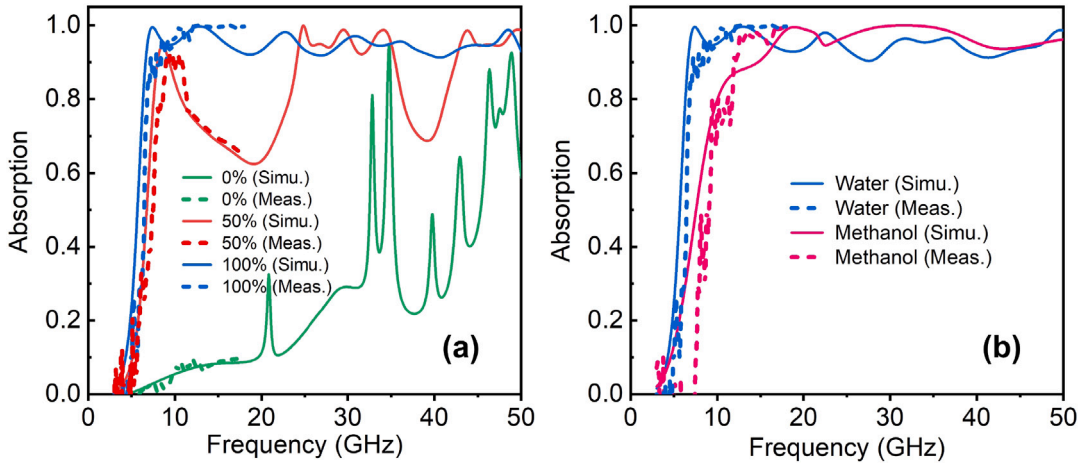

Fig. 12. The simulated and measured results of absorption spectra of the proposed UWBWMA with (a) different water levels and (b) different liquids.

Table 1
Performance comparison with previous water-based absorber works.

Ref.	Water container structure	Absorption band (GHz)	RBW (%)	Thickness (mm)	Incident angle stability (deg.)[a]
[25]	Irregular shape	6.8–21	101.9	10.4 (0.24λ_L)	30
[26]	I shape	7.9–21.7	93.2	5.8 (0.15λ_L)	30
[38]	Moth-eye shape	4–120	187	55 (0.73λ_L)	30
[39]	Cuboid shape	10.45–11.2	6.9	9 (0.31λ_L)	30
[40]	Block shape	7.74–23.56	101	12.8 (0.33λ_L)	30
[41]	Cross shape	7.28–28.22	117.9	6.5 (0.16λ_L)	30
[42]	Fabry–Perot cavity shape	260–30,000	196.5	0.096 (0.08λ_L)	NA
This work	Truncated cone shape	6.5–50.7	154.5	5.935 (0.13λ_L)	40

[a] Determined with absorptivity above 90% in both TE and TM modes.

angle insensitivity of the fabricated UWBWMA structure. Furthermore, the absorption performance of the fabricated sample is measured with different water levels of 0%, 50%, and 100% and various liquids of water and methanol, as shown in Fig. 12(a) and (b), respectively. As depicted in Fig. 12, the experiment results are nearly close to the simulation results. These obtained results confirm that the absorption performance of the proposed structure can change by tailoring the filled water levels and type of inside liquids. However, it can be seen that the left edge spectrum and absorption efficiency of measured results are slightly shifted compared with simulation results. Experimental factors, such as the size limitation of the fabricated sample and the influence of manufacturing errors as considered above, are responsible for the slight difference observed between the simulation and measurement.

Finally, the properties of the previously reported water-based absorber structures are summarized in Table 1. The absorber characteristics are in terms of shape structure, absorption band with efficiency above 90%, RBW, thickness, and incident angle stability. From Table 1, compared with the absorbers operated in the microwave region, the proposed structure achieves the thinnest structural thickness and widest incident angle stability while keeping a moderate RBW. Compared with the metasurface absorber in [38], the proposed absorber has a little bit narrower RBW than the Ref. [38], however, it has a much thinner thickness (around 1/6) than [38] and increases incident angle stability (around 33%).

5. Conclusion

A high-efficiency and ultra-wideband water-based metasurface absorber using 3D printing was proposed. The proposed 3D-printed UWBWMA achieved over 90% absorption in the range of 6.5–50.7 GHz. Furthermore, the designed UWBWMA exhibited excellent thermal stability, a wide incident angle insensitivity, and polarization-independent characteristics. Importantly, the absorption response of the UWBWMA could be tuned by controlling the filled water content and type of inside liquids, while maintained for various PLA resins of commercial 3D printing. The performance of the proposed structure was verified by experiment, which showed a good agreement with the simulation result. By virtue of the advantages of the proposed UWBWMA, it offers great promising applications such as EM stealth and radiation protection.

CRediT authorship contribution statement

Huu Lam Phan: Writing – review & editing, Writing – original draft, Validation, Investigation, Formal analysis. **Dac Tuyen Le:** Writing – review & editing, Investigation, Formal analysis, Data curation. **Xuan Khuyen Bui:** Writing – review & editing, Investigation, Formal analysis, Data curation. **Dinh Lam Vu:** Writing – review & editing, Validation. **Hong Quang Nguyen:** Writing – review & editing, Investigation, Formal analysis, Data curation. **Ngoc Huyen Duong:** Writing – review & editing, Validation. **Thi Minh Nguyen:** Writing – review & editing, Investigation, Formal analysis. **Thi Quynh Hoa Nguyen:** Writing – review & editing, Writing – original draft, Supervision, Funding acquisition, Conceptualization. **Jung-Mu Kim:** Writing – review & editing, Writing – original draft, Validation.

Declaration of competing interest

We know of no conflict of interest associated with this publication, and there hat been no significant financial support for this work that could have influenced its outcome.

Data availability

No data was used for the research described in the article.

Acknowledgments

This research is funded by Vietnam National Foundation for Science and Technology Development (NAFOSTED) under grant number 103.02-2021.44.

References

[1] P. Sahoo, L. Saini, A. Dixit, Microwave-absorbing materials for stealth application: a holistic overview, Oxf. Open Mater. Sci. 3 (1) (2022).
[2] D. Wu, C. Liu, Z. Xu, Y. Liu, Z. Yu, L. Yu, L. Chen, R. Li, R. Ma, H. Ye, The design of ultra-broadband selective near-perfect absorber based on photonic structures to achieve near-ideal daytime radiative cooling, Mater. Des. 139 (2018) 104–111.
[3] Q. Zhou, X. Yin, F. Ye, X. Liu, L. Cheng, L. Zhang, A novel two-layer periodic stepped structure for effective broadband radar electromagnetic absorption, Mater. Des. 123 (2017) 46–53.
[4] Z. Wang, Y. Wei, C. Zhang, Flexible broadband absorber for solar energy harvesting, Plasmonics (2023).
[5] S. Li, L. Liu, Y. Jiang, C. Tang, C. Gu, Z. Li, Ultrathin optically transparent metamaterial absorber for broadband microwave invisibility of solar panels, J. Phys. D: Appl. Phys. 55 (4) (2021) 045101.
[6] Y. Matsuno, A. Sakurai, Perfect infrared absorber and emitter based on a large-area metasurface, Opt. Mater. Express 7 (2) (2017) 618.
[7] P. Yin, L. Zhang, P. Sun, J. Wang, X. Feng, Y. Zhang, J. Dai, Y. Tang, Apium-derived biochar loaded with MnFe2o4@C for excellent low frequency electromagnetic wave absorption, Ceram. Int. 46 (9) (2020) 13641–13650.
[8] J. Jung, H. Park, J. Park, T. Chang, J. Shin, Broadband metamaterials and metasurfaces: a review from the perspectives of materials and devices, Nanophotonics (ISSN: 2192-8606) 9 (10) (2020) 3165–3196.
[9] N.I. Landy, S. Sajuyigbe, J.J. Mock, D.R. Smith, W.J. Padilla, Perfect metamaterial absorber, Phys. Rev. Lett. 100 (20) (2008).
[10] Y. Liu, S. Gu, C. Luo, X. Zhao, Ultra-thin broadband metamaterial absorber, Appl. Phys. A (ISSN: 1432-0630) 108 (1) (2012) 19–24.
[11] P.V. Tuong, J.W. Park, J.Y. Rhee, K.W. Kim, W.H. Jang, H. Cheong, Y.P. Lee, Polarization-insensitive and polarization-controlled dual-band absorption in metamaterials, Appl. Phys. Lett. 102 (8) (2013).
[12] W. Zhu, Y. Huang, I.D. Rukhlenko, G. Wen, M. Premaratne, Configurable metamaterial absorber with pseudo wideband spectrum, Opt. Express (ISSN: 1094-4087) 20 (6) (2012) 6616.
[13] Y. Cui, K.H. Fung, J. Xu, H. Ma, Y. Jin, S. He, N.X. Fang, Ultrabroadband light absorption by a sawtooth anisotropic metamaterial slab, Nano Lett. (ISSN: 1530-6992) 12 (3) (2012) 1443–1447.
[14] C. Long, S. Yin, W. Wang, W. Li, J. Zhu, J. Guan, Broadening the absorption bandwidth of metamaterial absorbers by transverse magnetic harmonics of 210 mode, Sci. Rep. (ISSN: 2045-2322) 6 (1) (2016).
[15] N.T.Q. Hoa, P.H. Lam, P.D. Tung, Wide-angle and polarization-independent broadband microwave metamaterial absorber, Microw. Opt. Technol. Lett. 59 (5) (2017) 1157–1161.
[16] W. Ma, Y. Wen, X. Yu, Broadband metamaterial absorber at mid-infrared using multiplexed cross resonators, Opt. Express (ISSN: 1094-4087) 21 (25) (2013) 30724.
[17] C. Gong, M. Zhan, J. Yang, Z. Wang, H. Liu, Y. Zhao, W. Liu, Broadband terahertz metamaterial absorber based on sectional asymmetric structures, Sci. Rep. (ISSN: 2045-2322) 6 (1) (2016).
[18] T.K.T. Nguyen, T.N. Cao, N.H. Nguyen, L.D. Tuyen, X.K. Bui, C.L. Truong, D.L. Vu, T.Q.H. Nguyen, Simple design of a wideband and wide-angle insensitive metamaterial absorber using lumped resistors for X- and Ku-bands, IEEE Photonics J. (ISSN: 1943-0647) 13 (3) (2021) 1–10.
[19] X. Zhang, F. Yan, X. Du, W. Wang, M. Zhang, Broadband water-based metamaterial absorber with wide angle and thermal stability, AIP Adv. (ISSN: 2158-3226) 10 (5) (2020).
[20] Z. Ma, C. Jiang, J. Li, X. Huang, A high absorptance wide-band metamaterial absorber with metasurface and low-permittivity dielectric slabs, J. Phys. D: Appl. Phys. (ISSN: 1361-6463) 55 (48) (2022) 485501.
[21] R.E. Jacobsen, S. Arslanagić, A.V. Lavrinenko, Water-based devices for advanced control of electromagnetic waves, Appl. Phys. Rev. (ISSN: 1931-9401) 8 (4) (2021).
[22] M. Cao, X. Huang, L. Gao, X. Li, L. Guo, H. Yang, Broadband bi-directional all-dielectric transparent metamaterial absorber, Nanomaterials 12 (23) (2022) 4124.
[23] Y.J. Yoo, S. Ju, S.Y. Park, Y. Ju Kim, J. Bong, T. Lim, K.W. Kim, J.Y. Rhee, Y. Lee, Metamaterial absorber for electromagnetic waves in periodic water droplets, Sci. Rep. (ISSN: 2045-2322) 5 (1) (2015).
[24] X. Huang, H. Yang, Z. Shen, J. Chen, H. Lin, Z. Yu, Water-injected all-dielectric ultra-wideband and prominent oblique incidence metamaterial absorber in microwave regime, J. Phys. D: Appl. Phys. (ISSN: 1361-6463) 50 (38) (2017) 385304.
[25] Z. Shen, X. Huang, H. Yang, T. Xiang, C. Wang, Z. Yu, J. Wu, An ultra-wideband, polarization insensitive, and wide incident angle absorber based on an irregular metamaterial structure with layers of water, J. Appl. Phys. 123 (22) (2018).
[26] Y. Zhou, Z. Shen, X. Huang, J. Wu, Y. Li, S. Huang, H. Yang, Ultra-wideband water-based metamaterial absorber with temperature insensitivity, Phys. Lett. A 383 (23) (2019) 2739–2743.
[27] X. Zhang, D. Zhang, Y. Fu, S. Li, Y. Wei, K. Chen, X. Wang, S. Zhuang, 3-D printed swastika-shaped ultrabroadband water-based microwave absorber, IEEE Antennas Wirel. Propag. Lett. (ISSN: 1548-5757) 19 (5) (2020) 821–825.
[28] A. Andryieuski, S.M. Kuznetsova, S.V. Zhukovsky, Y.S. Kivshar, A.V. Lavrinenko, Water: Promising opportunities for tunable all-dielectric electromagnetic metamaterials, Sci. Rep. (ISSN: 2045-2322) 5 (1) (2015).
[29] J. Wen, Q. Zhao, R. Peng, H. Yao, Y. Qing, J. Yin, Q. Ren, Progress in water-based metamaterial absorbers: a review, Opt. Mater. Express 12 (4) (2022) 1461.
[30] T.Q.M. Nguyen, T.K.T. Nguyen, D.T. Le, C.L. Truong, D.L. Vu, T.Q.H. Nguyen, Numerical study of an ultra-broadband and wide-angle insensitive perfect metamaterial absorber in the UV–NIR region, Plasmonics (ISSN: 1557-1963) 16 (5) (2021) 1583–1592.
[31] J. Ge, Y. Zhang, H. Li, H. Dong, L. Zhang, Ultra-broadband, tunable, and transparent microwave meta-absorber using ITO and water substrate, Adv. Opt. Mater. (ISSN: 2195-1071) 11 (10) (2023).
[32] D. Smith, D. Vier, T. Koschny, C. Soukoulis, Electromagnetic parameter retrieval from inhomogeneous metamaterials, Phys. Rev. E (ISSN: 1539-3755) 71 (3, 2) (2005).
[33] D.T. Phan, T.K.T. Nguyen, N.H. Nguyen, D.T. Le, X.K. Bui, D.L. Vu, C.L. Truong, T.Q.H. Nguyen, Lightweight, ultra-wideband, and polarization-insensitive metamaterial absorber using a multilayer dielectric structure for C- and X-Band applications, Phys. Status Solidi (b) 258 (10) (2021) 2100175.
[34] T.M. Nguyen, D.L. Vu, T.Q.H. Nguyen, J.-M. Kim, Reconfigurable broadband metasurfaces with nearly perfect absorption and high efficiency polarization conversion in THz range, Sci. Rep. (ISSN: 2045-2322) 12 (1) (2022).
[35] X. Fang, W. Li, X. Chen, Z. Wu, Z. Zhang, Y. Zou, Controlling the microstructure of biomass-derived porous carbon to assemble structural absorber for broadening bandwidth, Carbon (ISSN: 0008-6223) 198 (2022) 70–79.
[36] J. Luo, S. Qiao, Y. Tan, X. Fang, Z. Wu, Y. Zeng, Y. Yang, X. Chen, Y. Zou, An ultra-broadband lightweight structural absorber with excellent absorption enhancement based on traditional carbon-based absorbents, Carbon (ISSN: 0008-6223) 214 (2023) 118269.
[37] J. Luo, X. Chen, Z. Wu, Z. Zhang, Y. Zou, A cubic array structure with enhanced absorption bandwidth, Opt. Commun. (ISSN: 0030-4018) 474 (2020) 126176.
[38] H. Kwon, G. D'Aguanno, A. Alú, Optically transparent microwave absorber based on water-based moth-eye structures, Opt. Express (ISSN: 1094-4087) 29 (6) (2021) 9190.
[39] Q. Wang, K. Bi, S. Lim, All-dielectric transparent metamaterial absorber with encapsulated water, IEEE Access 8 (2020) 175998–176004.
[40] J. Xie, S. Quader, F. Xiao, C. He, X. Liang, J. Geng, R. Jin, W. Zhu, I.D. Rukhlenko, Truly all-dielectric ultrabroadband metamaterial absorber: Water-based and ground-free, IEEE Antennas Wirel. Propag. Lett. 18 (3) (2019) 536–540.
[41] Y. Lu, J. Chen, J. Li, Design of all-dielectric ultra-wideband transparent water-based absorber, J. Phys. D: Appl. Phys. 55 (11) (2021) 115502.
[42] Z. Zhong, Q. Wu, F. Ling, B. Zhang, Method for designing ultra-wideband absorbers based on water-filled Fabry–Perot cavity with continuously varying cavity length, Opt. Lett. 48 (21) (2023) 5591–5594.